



CrossMark  
click for updates

Cite this: *RSC Adv.*, 2015, 5, 48626

Received 4th May 2015  
Accepted 26th May 2015

DOI: 10.1039/c5ra08202a

www.rsc.org/advances

## Adhesion promoter for a multi-dielectric-layer on a digital microfluidic chip†

Jie Gao,<sup>a</sup> Tianlan Chen,<sup>a</sup> Cheng Dong,<sup>a</sup> Yanwei Jia,<sup>a</sup> Pui-In Mak,<sup>\*a</sup> Mang-I. Vai<sup>a</sup> and Rui P. Martins<sup>ab</sup>

A silane-based adhesion promoter suitable for a multi-dielectric-layer coating on a digital microfluidic chip is reported. It measures >100× improvement in chip lifetime *via* transforming the bonding of the dielectric layers (Ta<sub>2</sub>O<sub>5</sub> and Parylene C) from nonspecific to chemical. The refined chip-fabrication protocol also allows low EWOD actuation voltages down to 5 V.

### 1 Introduction

Digital microfluidics (DMF) is an electronic droplet-control technology based on the principle of electrowetting-on-dielectric (EWOD). In a DMF system, droplets sit on an electrode array coated with a dielectric layer followed by a layer of an inert hydrophobic material.<sup>1</sup> When a droplet covers two electrodes where one is charged, the contact angle of the droplet would be out of balance, *i.e.* a bigger contact angle on the uncharged electrode and smaller contact angle on the charged one. The droplet would move from the uncharged to the charged electrode in order to lower its surface energy. By this means, droplets containing biochemical samples can be transported, dispensed, mixed and stored on chip as desired by charging different electrodes.<sup>2–4</sup>

Due to the flexibility of DMF in manipulating individual droplets in nanoliter volume, different biological and chemical micro-reactions such as molecular probes synthesis,<sup>5</sup> proteomics,<sup>6</sup> immunoassays,<sup>7</sup> DNA sample processing<sup>8</sup> and cell-based assays<sup>9</sup> have been successfully run on DMF chips.<sup>10</sup> Yet, all those investigations entailed an actuation voltage as high as 100 V to execute droplet operations, which greatly raised the cost of the control electronics.

In order to lower the driving voltage to be compatible with the low-cost control electronics, researchers have tried different methods. According to the Young–Lippmann equation,<sup>11</sup> the contact angle of a droplet on an electrode applied with a certain voltage  $V$  follows

$$V^2 = [\cos \theta(V) - \cos \theta(0)]2t\gamma_{lg}/\epsilon_r\epsilon_0 \quad (1)$$

where  $\epsilon_r$  is the relative dielectric constant,  $\gamma_{lg}$  is the liquid–gas interface tension,  $t$  is the thickness of the dielectric layer,  $\theta(0)$  is the contact angle without electric field, and  $\theta(V)$  is the contact angle at a voltage  $V$ . To actuate a droplet from still, the contact angle difference with and without charging has to be larger than a threshold. For example, on a typical Teflon coated surface, a change of contact angle from 120° to <80° is entailed.<sup>12</sup> This sets a threshold in driving voltage to actuate a droplet.

To lower the driving voltage, we could either reduce the dielectric layer thickness  $t$  or increase the relative dielectric constant  $\epsilon_r$ . By reducing the dielectric layer thickness, Pollack *et al.*<sup>13</sup> has fabricated a DMF chip with 800 nm Parylene C as the dielectric layer and 60 nm Teflon as the hydrophobic surface to achieve a driving voltage of 80 V. Cho *et al.*<sup>14</sup> coated a chip with 100 nm silicon dioxide (SiO<sub>2</sub>) and 20 nm Teflon to further lower the driving voltage to 25 V. Regrettably, these thin film approaches are more susceptible to electric breakdown due to the possible imperfections within the films.

Instead of decreasing the dielectric thickness,  $t$ , people also investigated high dielectric constant materials such as Barium Strontium Titanate (BST,  $\epsilon_r \approx 300$ )<sup>15</sup> and aluminum oxide (Al<sub>2</sub>O<sub>3</sub>,  $\epsilon_r \approx 10$ ).<sup>16</sup> Nevertheless, these materials normally require high annealing temperature (~700 °C), which may soften or melt the typical glass substrate of DMF systems. Lin's group<sup>17</sup> has implemented multi-dielectric layers consisting of tantalum pentoxide (Ta<sub>2</sub>O<sub>5</sub>,  $\epsilon_r \approx 20$ ) annealed under 400 °C and Parylene C on glass substrate, where the latter can freely fill in the tiny cracks or pinholes within the former. However, Parylene C, through its deposition process, does not adhere chemically but nonspecifically to the substrate due to the great chemical dissimilarities

<sup>a</sup>State Key Laboratory of Analog and Mixed-Signal VLSI and FST-ECE, University of Macau, Avenida da Universidade, Taipa, Macao SAR, China. E-mail: pimak@umac.mo; Fax: +853-2882-2441; Tel: +853-8822-8796

<sup>b</sup>On leave from Instituto Superior Técnico, Universidade de Lisboa, Portugal

† Electronic supplementary information (ESI) available: (1) a video demo – the electrode lifetime testing. See DOI: 10.1039/c5ra08202a

between the two surfaces.<sup>18</sup> Additionally, the lifetime of the dielectric layer was often limited<sup>19</sup> or questioned.<sup>17,20</sup>

In this work, we introduce methacryloxypropyltrimethoxy-silane (A-174) as an the adhesion promoter in the coating process of multi-dielectric layers, Ta<sub>2</sub>O<sub>5</sub> and Parylene C, to form chemical bonds across the interface, differing from the typical single dielectric layer of Parylene C with A-174. The electrode lifetime is elongated by >100 times, and the EWOD actuation voltage can be as low as 5 V.

## 2 Materials and method

The DMF chip fabrication procedure is depicted in Fig. 1. The Cr electrodes on the bottom plate were patterned on a B-270 glass (Changsha Shaoguang Chrome Blank, SG2506) with standard lithographical and wet-etch methods (step 1–2). Then, the Ta<sub>2</sub>O<sub>5</sub> dielectric layer was deposited by reactive DC magnetron sputtering (HHV, Auto 500) at room temperature with a 99.99% Ta (Kurt J. Lesker) target under an Ar/O<sub>2</sub> ambient (15 sccm Ar and 2.05 sccm O<sub>2</sub>) with a working pressure of  $1.3 \times 10^{-4}$  Pa. Various thicknesses Ta<sub>2</sub>O<sub>5</sub> layers were obtained by regulating the sputtering time. The oxidized layer was rapidly thermal annealed in a N<sub>2</sub> atmosphere (20 sccm) at 400 °C for 10 min to reduce the number of pinholes in the dielectric layer. In step 4, the surface of the obtained chip was primed with A-174 silane (Momentive Performance Materials) in isopropyl alcohol (1%, v/v) for 15 min and baked at 120 °C for 5 min. Low pressure chemical vapor deposition method (La-Chi, LH300) was then adopted to deposit Parylene-C layer (360 nm) on top of Ta<sub>2</sub>O<sub>5</sub> surface in step 5. This extra layer covered the pinholes in Ta<sub>2</sub>O<sub>5</sub> layer preventing their exposure to liquid samples while maintaining the high dielectric constant and the strength of the Ta<sub>2</sub>O<sub>5</sub>. At last (step 6), 100 nm fluoropolymer hydrophobic layer was spin coated with 0.5% Teflon® AF (1601S, Dupont) in per-fluorosilane (FC-40, 3M) at 3200 rpm for 60 s and baked at 160 °C for 4 hours. The top plate was an ITO glass coated with Teflon following the same protocol as for the bottom plate (steps 7–8). In step 9, a droplet was dispensed with a pipette and sandwiched in silicon oil (1 cSt, Clearco) between the two plates assembled with a spacer.

The setup of the Digital Microfluidic system was the same as previously described.<sup>21–23</sup> Briefly, as shown in Fig. 2, there were

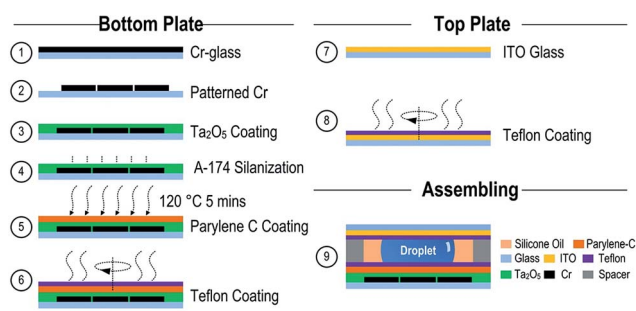


Fig. 1 Fabrication procedure of Ta<sub>2</sub>O<sub>5</sub> and Parylene C insulated two-plate DMF chip.

four parts in the system: a DMF chip, an electronic control panel, a field-programmable gate array (FPGA) board and a software control program. The charging and discharging of the electrodes on the DMF chip were controlled through an electronic printed circuit board (PCB) *via* the FPGA. The internal units of the FPGA preceded the data transfer, frequency detection, data collection and operation controller. A user friendly and upgradable human-controlled interface was installed in a PC and connected to the system for the entire module management. The driving signal was a 1 kHz square wave supported by a low-cost signal generator (GFG-8255A Instek®).

## 3 Results and discussion

### 3.1 Structure of the Ta<sub>2</sub>O<sub>5</sub> dielectric layer

The dielectric permittivity of a thin dielectric film depends not only on the material, but also on its crystal structure. According to Chiu,<sup>24</sup> amorphous Ta<sub>2</sub>O<sub>5</sub> exhibited a much lower leakage current than crystallized Ta<sub>2</sub>O<sub>5</sub>. That could help to raise the break-down voltage, and therefore improve the robustness of the DMF chip. In this work, the Ta<sub>2</sub>O<sub>5</sub> thin films were rapidly thermal annealed in N<sub>2</sub> atmosphere at 400 °C for 10 min at a ramp of 100 °C min<sup>-1</sup> to guarantee the hardness of the substrate. X-ray diffraction (XRD) as shown in Fig. 3 clearly demonstrated a typical hump between 2θ angle of 20° and 30°, indicating the amorphous structure of the Ta<sub>2</sub>O<sub>5</sub> thin film. As the leakage current increases with the increase of surface roughness,<sup>25</sup> a smooth surface/interface could enhance the dielectric strength and decrease the possibility of dielectric breakdown. The roughness of the Ta<sub>2</sub>O<sub>5</sub> films was characterized by Atomic Force Microscope (AFM) and shown in the sub-image of Fig. 3. The measured root mean square roughness was 0.75 nm over a 1.5 μm × 1.5 μm surface of a 100 nm thick film. This was widely accepted as very smooth and homogeneous, which would also increase the dielectric strength due to the limited leakage current.

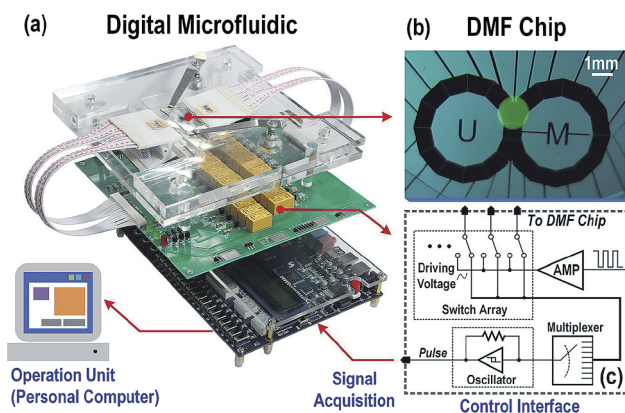


Fig. 2 Setup of the control-engaged DMF system. (a) The DMF module consists of four operation parts: the chip holder, the control electronics layer, the field-programmable gate array (FPGA) board and the software control program. (b) The fabricated DMF chip. (c) The control electronics for real-time droplet actuation and sensing.

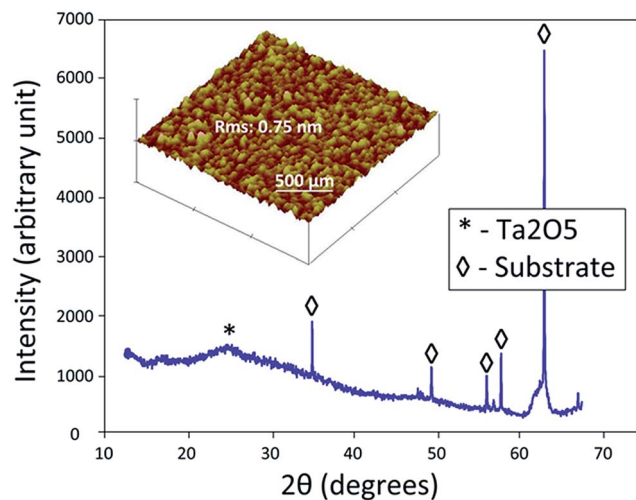


Fig. 3 X-ray diffraction (XRD) pattern of rapidly thermal annealed (RTA) Ta<sub>2</sub>O<sub>5</sub> thin film at 400 °C for 10 min in N<sub>2</sub> atmosphere. Insert: topographic image characterized by atomic force microscopy (AFM).

### 3.2. A-174 silane as an adhesion promoter

As we have mentioned above, Parylene C does not adhere chemically but nonspecifically to Ta<sub>2</sub>O<sub>5</sub> thin film, causing its peeling off and breakdown of the dielectric layers. A-174 has been proven to promote strong adhesion between Parylene-C and the substrate.<sup>26</sup> In order to improve the adhesion between Parylene C and Ta<sub>2</sub>O<sub>5</sub>, we utilized A-174 silane as a bonding promoter.

Fig. 4 shows the schematic principle of A-174 as an adhesion promoter. A-174 is composed of two functional groups, a methoxy silane head and a methacryloxy tail (Fig. 4a). Parylene C stays as dimer in powder and breaks into monomers in air when evaporated (Fig. 4b). During the coating process, the surface of Ta<sub>2</sub>O<sub>5</sub> would react with adsorbed water molecules in air and form a hydroxyl group, Ta-OH.<sup>27</sup> This hydroxyl group has the ability to react with the methoxy silane head of A-174 forming a self-limited A-174 molecular layer on the Ta<sub>2</sub>O<sub>5</sub> surface (Fig. 4c). When deposited on the A-174 modified Ta<sub>2</sub>O<sub>5</sub> surface, monomers of Parylene C (Fig. 4b) would co-polymerize with the methacryloxy tail of A-174 *via* a free radical addition reaction and deposit as a polymer layer.<sup>28–30</sup> By this way, the nonspecific adhesion between the two dielectric layers, Ta<sub>2</sub>O<sub>5</sub> and Parylene C, would be switched to a much stronger and stable chemical bonding.

In order to further investigate the influence of the silanization on the robustness of the DMF chip, chips fabricated with and without A-174 were compared side by side to shuttle a droplet of DI water from one electrode to the next under the same actuation voltage. The electrode lifetime was determined when an electrode breakdown was observed. The droplet may still be movable in some cases. The film thicknesses of Ta<sub>2</sub>O<sub>5</sub>, Parylene-C and Teflon were 250 nm, 480 nm and 100 nm, respectively. The spacer between the top and bottom plates was set as 300 μm. A droplets (0.65 μL) was driven either by 15 V AC or DC actuation signals. The charging duration was set empirically at 400 ms. A video of these experiments can be found in ESM\_1.

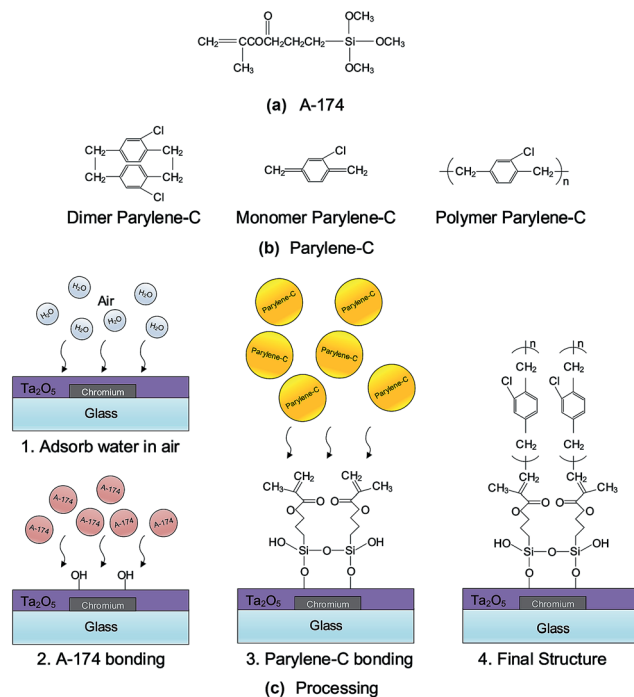


Fig. 4 Schematics of A-174 promoting adhesion between Ta<sub>2</sub>O<sub>5</sub> and Parylene C. (a) Chemical structure of A-174; (b) chemical structure of dimer, monomer and polymer Parylene-C; (c) bonding process of Ta<sub>2</sub>O<sub>5</sub> and Parylene-C.

As shown in Fig. 5a and b, without A-174 silanization the Parylene-C layer peeled off the substrate even on some freshly fabricated chips, while with A-174 the Parylene-C stuck well to the substrate. As a consequence, the electrodes easily broke down without silanization [Fig. 5c] while no sign of breakdown was observed on silanized chips after 10 000 shuttles of a droplet actuation [Fig. 5d]. The statistical lifetime of different chips driven by DC or AC is shown in Fig. 5e. With the A-174 silanization treatment, the dielectric layers successfully protected the electrodes. No matter what actuation signal was used, the chips were robust enough to survive at least 10 000 shuttles of droplet movement. Note that the lifetime was actually even longer as we stopped our program at 10 000 shuttles where the chips were still in excellent condition. For the untreated chips, the electrode broke down in less than 10 shuttles driven by DC. Although AC worked more gently on the chip, it only improved the lifetime to around 400 shuttles. In average, the electrode lifetime was elongated over 100 times by utilizing A-174 silanization treatment. The chip reliability was significantly improved demonstrated by the elongated electrode lifetime.

### 3.3. Droplet transportation velocity in relation to the thickness of dielectric layer

The limited actuation voltage and movement velocity of a droplet transportation in DMF have hindered it from high throughput applications.<sup>31–33</sup> As reported, the droplet transportation's velocity depends on the actuation voltage, the size of the droplet and the electrode-driving signals.<sup>21</sup> Here the robust

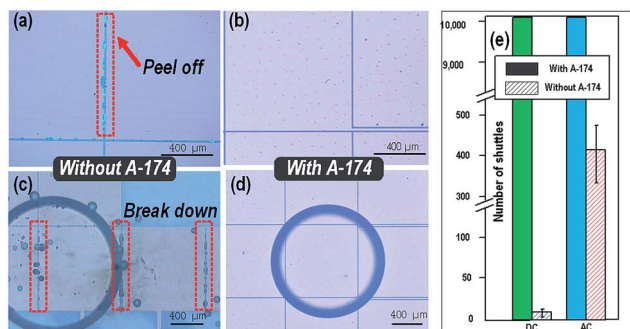


Fig. 5 Topographic images of DMF chips coated with Ta<sub>2</sub>O<sub>5</sub> and Parylene C with and without A-174 as an adhesion promoter. (a) Freshly fabricated chip without A-174. (b) Freshly fabricated chip with A-174. (c) After running droplets on chip without A-174, (d) After running droplets on chip with A-174.

chip coated with multi-dielectric-layer treated with A-174 provides the opportunity for us to study the lowest limit of the actuation voltage and the relationship between the droplet velocity and the dielectric layer thickness for the first time.

As shown in Fig. 6, the threshold of the driving voltage to kick off a droplet from still depended on the thickness of Ta<sub>2</sub>O<sub>5</sub>. For a 65 nm Ta<sub>2</sub>O<sub>5</sub> layer, the threshold was 5 V, while for Ta<sub>2</sub>O<sub>5</sub> layers of 115 nm and 180 nm, the threshold was 10 V. The lowest actuation voltage from the literature was 7.2 V with a 135 nm Ta<sub>2</sub>O<sub>5</sub>, 180 nm Parylene C and 70 nm of CYTOP ( $\epsilon_r \approx 2$ ) hydrophobic layer recipe.<sup>34</sup> Here, the threshold was pushed down to 5 V, 30% lower than reported. The thinner Ta<sub>2</sub>O<sub>5</sub> layer used in our study might be the reason to reduce the actuation voltage. Simultaneously, the thick Parylene C (360 nm) and

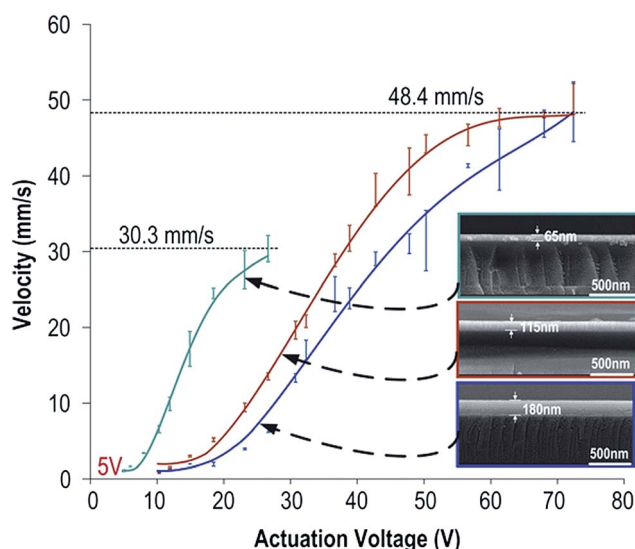


Fig. 6 Droplet transportation velocity as a function of the actuation voltage on chips with different thickness of Ta<sub>2</sub>O<sub>5</sub> layers. Insert: scanning electron microscope (SEM) cross-section micrographs of different thickness of Ta<sub>2</sub>O<sub>5</sub> thin films. The velocity was an average of a droplet moving across 12 electrodes. All experiments have been repeated for three times.

Teflon (100 nm) films helped improving the chip reliability. Furthermore, the velocity of the droplet transportation was higher with thinner Ta<sub>2</sub>O<sub>5</sub> layer under the same driving voltage due to the higher electric field strength. However, thicker dielectric layer sustained a higher breakdown voltage. As illustrated in Fig. 6, the chips with 115 nm and 180 nm Ta<sub>2</sub>O<sub>5</sub> did not break down at 72 V, the maximum voltage that our power supply could generate. The droplet transportation reached 48.4 mm s<sup>-1</sup> at 72 V, which was also higher than the reported value of 40 mm s<sup>-1</sup>.<sup>35</sup>

## 4 Conclusions

A-174 silane as a low-cost adhesion promoter significantly improves the bonding between layers of dielectric Ta<sub>2</sub>O<sub>5</sub> and Parylene C. It successfully lowers the EWOD operating voltage, prevents the dielectric breakdown and provides reliable operations of the DMF platform. The actuation voltage can be as low as 5 V following the described fabrication protocols. The chip is highly robust surviving more than 10 000 shuttles of a droplet between two adjacent electrodes without any sign of dielectric breakdown. A low actuation voltage and a high driving speed together with a robust operation property would help the commercialization of DMF chips.

## Acknowledgements

This work was financially supported by the Macao Science and Technology Development Fund (FDCT) and the University of Macau under no. 033/2011/A2, 047/2014/A1 and the State- Key Lab Establishment Fund.

## Notes and references

- 1 M. Abdelgawad and A. R. Wheeler, *Microfluid. Nanofluid.*, 2007, **4**, 349–355.
- 2 K. Chakrabarty, R. B. Fair and J. Zeng, *IEEE Trans Comput Aided Des. Integrated Circ. Syst.*, 2010, **29**, 1001–1017.
- 3 S. C. C. Shih, R. Fobel, P. Kumar and A. R. Wheeler, *Lab Chip*, 2011, **11**, 535–540.
- 4 M. Chakraborty, A. Ghosh and S. Dasgupta, 2014, 1–19.
- 5 S. Park, Y. Zhang, S. Lin, T.-H. Wang and S. Yang, *Biotechnol. Adv.*, 2011, **29**, 830–839.
- 6 L. Malic, T. Veres and M. Tabrizian, *Biosens. Bioelectron.*, 2011, **26**, 2053–2059.
- 7 C. Peng, Z. Zhang, C.-J. C. J. Kim and Y. S. Ju, *Lab Chip*, 2014, **14**, 1117–1122.
- 8 H. Kim, M. S. Bartsch, R. F. Renzi, J. He, J. L. Van de Vreugde, M. R. Claudnic and K. D. Patel, *J. Lab. Autom.*, 2011, **16**, 405–414.
- 9 I. Barbulovic-Nad, H. Yang, P. S. Park and A. R. Wheeler, *Lab Chip*, 2008, **8**, 519–526.
- 10 R. B. Fair, *Microfluid. Nanofluid.*, 2007, **3**, 245–281.
- 11 B. Berge, *C. R. Acad. Sci.*, 1993, **317**, 157–163.
- 12 J. H. Song, R. Evans, Y.-Y. Lin, B.-N. Hsu and R. B. Fair, *Microfluid. Nanofluid.*, 2008, **7**, 75–89.

- 13 M. G. Pollack, D. Shenderov and R. B. Fair, *Lab Chip*, 2002, **2**, 96–101.
- 14 S. K. Cho, H. Moon and C. Kim, *J. Microelectromech. Syst.*, 2003, **12**, 70–80.
- 15 H. Moon, S. K. Cho, R. L. Garrell and C. J. Kim, *J. Appl. Phys.*, 2002, **92**, 4080–4087.
- 16 J. H. Chang, D. Y. Choi, S. Han and J. J. Pak, *Microfluid. Nanofluid.*, 2010, **8**, 269–273.
- 17 Y.-Y. Lin, E. R. F. Welch and R. B. Fair, *Sens. Actuators, B*, 2012, **173**, 338–345.
- 18 C. C. Centre, D. Zeniieh and A. Bajwa, *21st International Symposium on Plasma Chemistry*, Queensland, Australia, 2013, pp. 2–5.
- 19 M. Dhindsa, S. Kuiper and J. Heikenfeld, *Thin Solid Films*, 2011, **519**, 3346–3351.
- 20 Y. Li, W. Parkes, L. I. Haworth, A. A. Stokes, K. R. Muir, P. Li, A. J. Collin, N. G. Hutcheon, R. Henderson, B. Rae and A. J. Walton, *Solid-State Electron.*, 2008, **52**, 1382–1387.
- 21 C. Dong, T. Chen, J. Gao, Y. Jia, P.-I. Mak, M.-I. Vai and R. P. Martins, *Microfluid. Nanofluid.*, 2015, **18**, 673–683.
- 22 T. Chen, C. Dong, J. Gao, Y. Jia, P.-I. Mak, M.-I. Vai and R. P. Martins, *AIP Adv.*, 2014, **4**, 047129.
- 23 J. Gao, X. Liu, T. Chen, P.-I. Mak, Y. Du, M.-I. Vai, B. Lin and R. P. Martins, *Lab Chip*, 2013, **13**, 443–451.
- 24 F. Chiu, J. Wang, J. Y. Lee and S. C. Wu, *J. Appl. Phys.*, 1997, **81**, 6911–6915.
- 25 Y.-P. Zhao, G.-C. Wang, T.-M. Lu, G. Palasantzas and J. De Hosson, *Phys. Rev. B: Condens. Matter Mater. Phys.*, 1999, **60**, 9157–9164.
- 26 C. Hassler, R. P. Von Metzen, P. Ruther and T. Stieglitz, *J. Biomed. Mater. Res., Part B*, 2010, **93**, 266–274.
- 27 C. J. Mitchell, G.-R. Yang and J. J. Senkevich, *J. Adhes. Sci. Technol.*, 2006, **20**, 1637–1647.
- 28 D. Witters, N. Vergauwe, S. Vermeir, F. Ceyskens, S. Liekens, R. Puers and J. Lammertyn, *Lab Chip*, 2011, **11**, 2790–2794.
- 29 S. H. Au, P. Kumar and A. R. Wheeler, *Langmuir*, 2011, **27**, 8586–8594.
- 30 P. T. Kumar, K. Vriens, M. Cornaglia, M. Gijs, T. Kokalj, K. Thevissen, A. Geeraerd, B. P. A. Cammue, R. Puers and J. Lammertyn, *Lab Chip*, 2015, 16–18.
- 31 J.-C. Baret, O. J. Miller, V. Taly, M. Ryckelynck, A. El-Harrak, L. Frenz, C. Rick, M. L. Samuels, J. B. Hutchison, J. J. Agresti, D. R. Link, D. A. Weitz and A. D. Griffiths, *Lab Chip*, 2009, **9**, 1850–1858.
- 32 P. B. Gupta, T. T. Onder, G. Jiang, K. Tao, C. Kuperwasser, R. A. Weinberg and E. S. Lander, *Cell*, 2009, **138**, 645–659.
- 33 Y. Jia, P.-I. Mak, C. Massey, R. P. Martins and L. J. Wagh, *Lab Chip*, 2013, **13**, 4635–4641.
- 34 Y.-Y. Lin, R. D. Evans, E. Welch, B.-N. Hsu, A. C. Madison and R. B. Fair, *Sens. Actuators, B*, 2010, **150**, 465–470.
- 35 D. Brassard, L. Malic, F. Normandin, M. Tabrizian and T. Veres, *Lab Chip*, 2008, **8**, 1342–1349.